Low-energy-electron production after 2*p* ionization of argon clusters

Hironobu Fukuzawa,[1,2,*] Yiwen Li,[1,2] Daehyun You,[1,2] Yuta Sakakibara,[1,2] Syuhei Yamada,[1,2] Yuta Ito,[1,2] Tsukasa Takanashi,[1,2] Masaki Oura,[2] Norio Saito,[2,3] and Kiyoshi Ueda[1,2]

[1]*Institute of Multidisciplinary Research for Advanced Materials, Tohoku University, Sendai 980-8577, Japan*

[2]*RIKEN SPring-8 Center, Kouto 1-1-1, Sayo, Hyogo 679-5148, Japan*

[3]*National Institute of Advanced Industrial Science and Technology, NMIJ, Tsukuba 305-8568, Japan*

(Received 28 June 2018; revised manuscript received 10 January 2019; published 9 April 2019)

Irradiation of matter with x rays causes inner-shell ionization of atoms and molecules, followed by subsequent electronic relaxation leading to production of low-energy electrons. In this study we investigate the process of low-energy-electron production in Ar clusters by electron-ion multiple coincidence measurements. In addition to photoelectrons, low-energy electrons are observed after 2*p* ionization of argon clusters. We find that low-energy-electron production increases when the energy of photoelectrons exceeds the ionization potential of Ar. We experimentally identify the low-energy electrons produced by interatomic electronic decay processes and inelastic scattering of the photoelectrons and Auger electrons with the surrounding Ar atoms.

DOI: 10.1103/PhysRevA.99.042505

I. INTRODUCTION

When condensed matter is irradiated with x rays, the most likely process is inner-shell photoionization followed by the emission of Auger electrons [1]. Subsequent relaxation processes also lead to the production of low-energy electrons. Understanding the process of low-energy-electron production by x rays, which may cause damage to DNA, has always been a heated topic [2]. Low-energy electrons are conventionally believed to be secondary electrons produced by inelastic scattering collisions of photoelectrons or Auger electrons with the surroundings, i.e., electron collisional ionizations of the surroundings. Inelastic scattering is an elementary scattering process where an incident particle loses the kinetic energy. The incident particle concerned in the present study refers to an electron, the energy of which affects the probability of inelastic scattering. The surplus energy lost from the incident electron is transferred to producing a secondary electron.

In [3], a new relaxation mechanism was predicted theoretically whereby low-energy electrons are generated through interatomic electronic decay processes between an electronically excited ion and an environment and named intermolecular (or interatomic) Coulombic decay (ICD). When ICD occurs, excess energy is transferred from excited ions to their neighbors and a slow electron is emitted. Intermolecular (or interatomic) Coulombic decay is a typical phenomenon in loosely bound matter in which atoms and molecules are surrounded by neighbors. It has been studied theoretically [4] and experimentally [5] in various systems. Researchers even substantiated the scientific evidence of the existence of ICD in water [6,7]. However, quantitative investigations to evaluate contributions from inelastic scattering vs ICD are lacking.

In the present study, Ar clusters are used as target samples. The ICD in Ar dimers and trimers after inner-shell photoionization was experimentally observed in previous studies [8,9]. The probability of the emitted electrons to collide with surrounding atoms in a cluster increases with an increase in the number of atoms in the cluster. Thus, Ar clusters of sizes up to dozens of atoms may be an ideal example to investigate contributions from both ICD and inelastic scattering. In order to distinguish electrons emitted from Ar atoms and clusters, we have carried out electron-ion coincidence measurements. The photon energies were 258 and 268 eV, i.e., ∼10 and 20 eV above the Ar 2*p* ionization threshold, respectively. In the latter case, the photoelectrons can ionize neutral Ar, whereas in the former case, they cannot. Thus, we can identify the contributions from the photoelectron inelastic scattering by comparing results from both photon energies.

In Fig. 1, the presumed reactions that proceed in Ar clusters are explained in a model consisting of three Ar atoms. The sequential process starts with Ar 2*p* photoionization by soft x rays (step 1) and is followed by subsequent Auger decay (step 2). The ICD is the third step in the sequential process and produces one doubly charged Ar ion and one singly charged Ar ion in the cluster. When the doubly charged ion is produced in the cluster, charge separation proceeds via radiative charge transfer or charge transfer through nonadiabatic transitions resulting in two singly charged ions as observed in dimers [10,11]. Thus, the cluster eventually releases three singly charged Ar atoms after charge transfer and Coulomb explosion (step 4). Instead of ICD, another type of interatomic process, electron transfer mediated decay (ETMD) [12], may occur. During ETMD, an electron is transferred from a neighbor to a vacant orbital of ion, and a slow electron is emitted from the neighbor or another neighbor using the excess energy caused by the electron transfer. The ETMD is usually considered not to compete with ICD [12], but in some cases efficiently produces low-energy electrons [13,14]. Electron transfer mediated decay processes where three species participate, ETMD(3) (step 3′), might occur in the present

*fukuzawa@tohoku.ac.jp

 ©2019 American Physical Society

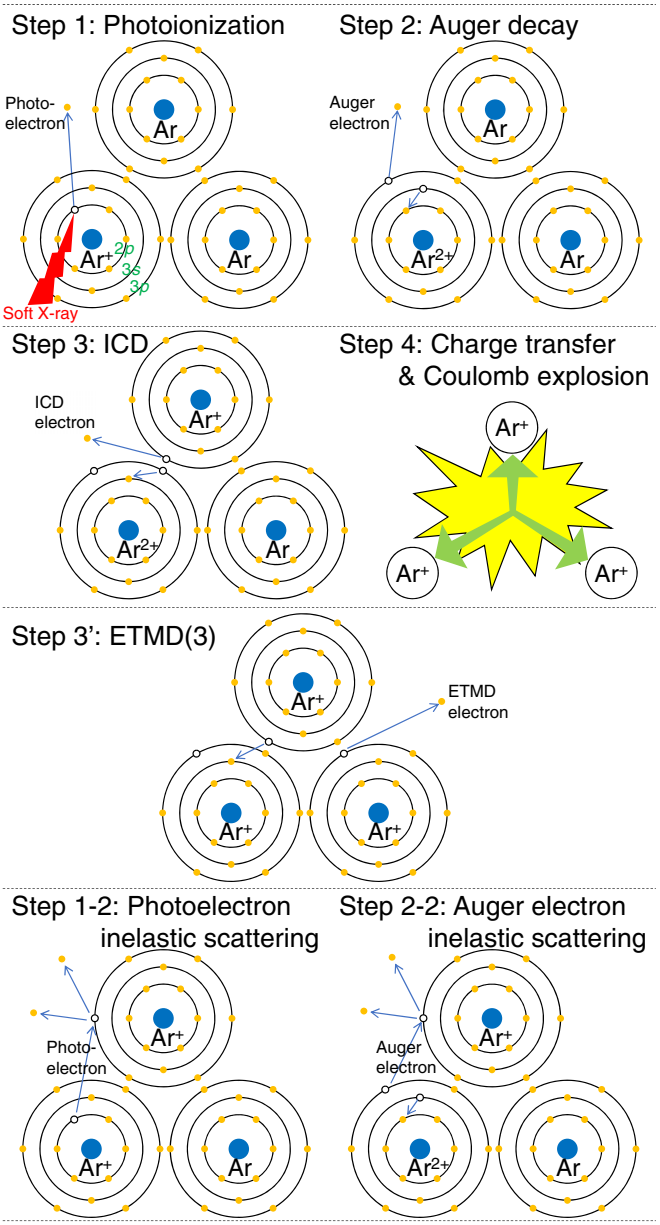

FIG. 1. Processes in the present study. Step 1 (photoionization): By irradiation of soft x rays, an inner $2p$ electron is emitted. Step 2 (Auger decay): A $3s$ electron makes a discrete transition to the vacant $2p$ electron shell. A bound $3p$ electron receives the energy gained in this process and escapes from the atom. Step 3 (ICD): An outer $3p$ electron fills the vacancy of the inner $3s$ shell. The excess energy is transferred to a neighboring Ar atom, which then emits an electron. Step 4 (charge transfer and Coulomb explosion): The triply charged cluster goes through charge transfer, leading to production of three singly charged atoms. The cluster eventually dissociates due to Coulomb force and releases three singly charged Ar atoms. Step $3'$ [ETMD(3)]: Instead of ICD, ETMD(3) may occur. In this process, an outer $3p$ electron of a neighboring Ar atom fills the vacancy of the inner $3s$ shell. The excess energy is transferred to another neighboring Ar atom, which then emits an electron. Step 1-2 (photoelectron inelastic scattering): When the photoelectron emitted in step 1 has enough energy to excite or ionize a neighboring Ar atom, inelastic scattering of the photoelectron by the neighboring atom occurs. Step 2-2 (Auger electron inelastic scattering): The Auger electron emitted in step 2 is scattered by the neighboring atom.

study since it may require lower energy than ICD where ICD is energetically forbidden. With regard to another possible pathway, after photoionization, inelastic scattering may take place when the photoelectrons have sufficient energy to excite or ionize other atoms shown as step 1-1. Inelastic scattering of Auger electrons is also possible (step 2-2) since Auger electrons generally have abundant energy.

II. EXPERIMENT

The experiment was performed at the b branch of the beamline BL17SU of SPring-8 in Japan [15]. The storage ring was operated in a mode of 53 single bunches plus 4/58 filling, alternately occupied by single bunches separated by 82.6 ns and a continuous bunch train in a period of 4×82.6 ns. Three-dimensional momenta of electrons and ions were measured in coincidence [16–18]. Two time-of-flight (TOF) spectrometers equipped with delay-line-type position-sensitive detectors were placed opposite to each other for detecting the electrons and ions simultaneously. For the ion spectrometer, the length of the first acceleration region was 16.5 mm and that of the second one was 82.5 mm. In the case of the electron spectrometer, there was only one acceleration region. In addition, there was a drift region after the acceleration region where there was no electric field. The lengths of the acceleration region and the drift region of the electron spectrometer were 33.0 and 67.4 mm, respectively. The TOF spectrometer for electrons was equipped with a hexagonal delay-line detector with an effective diameter of 120 mm, while that for the ions had an effective diameter of 80 mm. The static extraction field was set to be 1.7 V/mm. A uniform magnetic field of 6.8 G was superimposed to the spectrometer by a set of Helmholtz coils outside the vacuum chamber. In this experiment, the 4π collection efficiencies of electrons whose energies were below 26 eV were obtained. With the knowledge of detected position and arrival time at the detector, we are capable of extracting the information of three-dimensional momenta of each particle.

The cluster beam is introduced in the vertical direction into the chamber, while the soft x ray is introduced to the reaction point at a horizontal level. The Ar clusters were produced in a gas expansion through a nozzle. The diameter and the temperature of the nozzle were 30 μm and room temperature. The cluster beam was skimmed by a skimmer with a 0.5 mm diameter and an aperture with a 1 mm diameter before reaching the reaction point. Figure 2 shows the total ion yield (TIY) spectra measured under the two conditions where the stagnation pressures of Ar gases were 0.3 and 1.5 MPa. The TIY spectrum of 0.3 MPa is similar to the one of Ar atoms [19] and thus most of the species in the gas beam are isolated Ar atoms. In the TIY spectrum measured at 1.5 MPa, structures not seen in the spectrum at 0.3 MPa appear. These structures stem from clusters. For example, peaks at 244.7 and 245.2 eV stem from $2p_{3/2} \rightarrow 4s$ transitions of Ar on the surface and within the bulk of the argon clusters, respectively [20]. Using the areas of the peaks from the surfaces and the bulks at 244.7 and 245.2 eV, respectively, we estimated the average number of atoms in the cluster (averaged cluster size $\langle N \rangle$) to be ~70 atoms per cluster (see Appendix A for details). We adopted this method without relying on the size

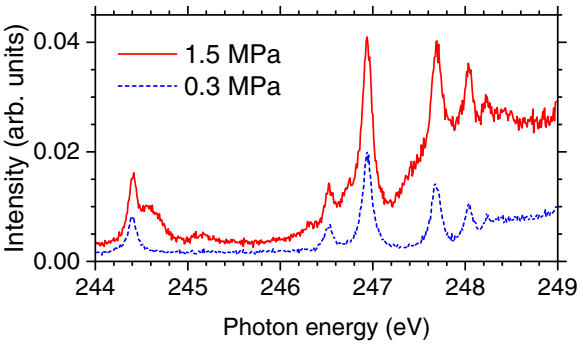

FIG. 2. Total ion yield spectra measured with 0.3 MPa (blue dashed line) and 1.5 MPa (red solid line) stagnation pressures of Ar gases.

distribution of final ion products because clusters cannot keep the size after core-level excitation or ionization.

III. RESULTS AND DISCUSSION

In the electron-ion coincidence experiments, the soft-x-ray photon energies were set to 258 and 268 eV, corresponding to 10 and 20 eV above the Ar 2p ionization threshold of 248 eV. Note that 10 and 20 eV are below and above the first ionization energy of neutral Ar. Ions produced by the soft-x-ray irradiation were accelerated by an electric field to the same kinetic energy as any other ions that have the same charge, and the ion-TOF spectra were measured. As depicted in Fig. 1, when ICD or ETMD or the photoelectron or Auger electron inelastic scattering occur, three singly charged ions are expected to be released via Coulomb explosion. To identify the electrons emitted from these processes, we selected events where three Ar^+ ions were detected in coincidence.

Figure 3 depicts electron spectra measured at 258- and 268-eV photon energies in coincidence with three Ar^+ ions

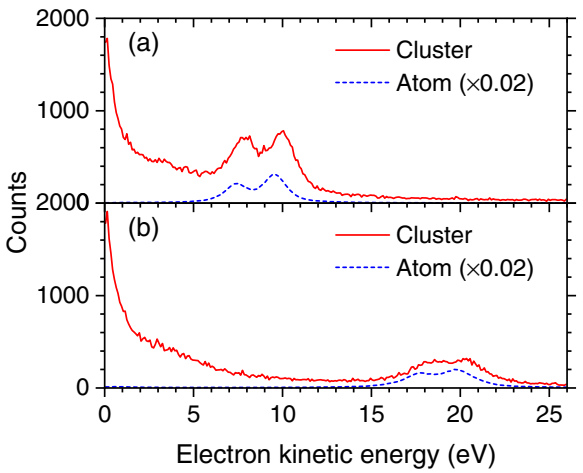

FIG. 3. Electron spectra for Ar clusters (red solid lines) and Ar atoms (blue dashed lines) measured at (a) 258-eV and (b) 268-eV photon energies. The spectra for clusters and atoms are measured simultaneously and obtained in coincidence with three Ar^+ and one Ar^{2+}, respectively. The bin size of the electron kinetic energy is 0.1 eV.

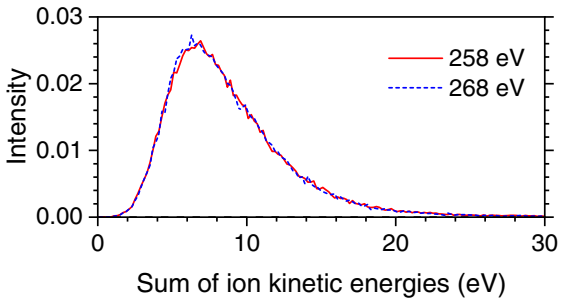

FIG. 4. Sum of kinetic energies of three Ar^+ ions measured at 258-eV (red solid line) and 268-eV (blue dashed line) photon energies. Intensities are obtained by dividing counts at each kinetic energy by the total counts (74 309 and 62 952 counts for 258 and 268 eV, respectively).

(red solid lines) and one nonenergetic Ar^{2+} ion (blue dashed lines). Electron spectra in coincidence with three Ar^+ ions originate from Ar clusters. On the other hand, electron spectra in coincidence with one nonenergetic Ar^{2+} ion are considered to arise from Ar atoms, since the Auger decay following the 2p ionization of Ar atoms produces nonenergetic Ar^{2+}. From the electron spectra for both clusters and atoms, we identified the evident Ar 2p photoelectron signals at ∼10 and ∼20 eV in the spectra measured at 258 and 268 eV, respectively. The two peaks separated ∼2 eV were assigned to be $2p_{1/2}$ (lower kinetic energy) and $2p_{3/2}$ (higher) photoelectrons. The peaks for clusters were slightly (∼0.5 eV) shifted towards the higher-kinetic-energy direction due to decrements of the ionization potential. Moreover, a gentle slope following the highest-energy limit (hereinafter called as slope 1) and a steep slope near zero-energy (hereinafter called as slope 2) were seen in the spectra for clusters at both photon energies. Since the kinetic energy of the Auger electrons emitted after Ar 2p ionization is ∼200 eV, the kinetic energy of electrons due to the Auger electron inelastic scattering may be distributed throughout the entire range of observed spectra. Thus we consider slope 1 to be due to the Auger electron inelastic scattering. The origin of slope 2 may be autoionization from vibrationally excited Rydberg states. Low-energy-electron emissions via this process are observed in the H_2 molecule [21].

Let us investigate the relationship between ion kinetic energies and electron spectra in order to understand the origin of each component. Figure 4 depicts distributions of the sum of kinetic energies of three Ar^+ ions. There is no significant difference in the distributions measured at different photon energies. The peak energy is ∼7 eV, whereas those from Ar_3 are ∼9 and 11 eV [9]. This indicates that distances between ions in Ar cluster in the present study are larger than those in Ar_3 when the Coulomb explosion occurs. On the other hand, the ions from the Ar cluster in this study are distributed over higher energy than from Ar_3. If each of the three Ar^+ ions is located at the site of Ar atoms in the neutral equilateral triangle Ar_3 with an internuclear distance of 3.8 Å [22], the Coulomb repulsion energy is ∼11 eV. The sum of three Ar^+ energies higher than ∼11 eV indicates that Ar cluster has a charge state higher than +3.

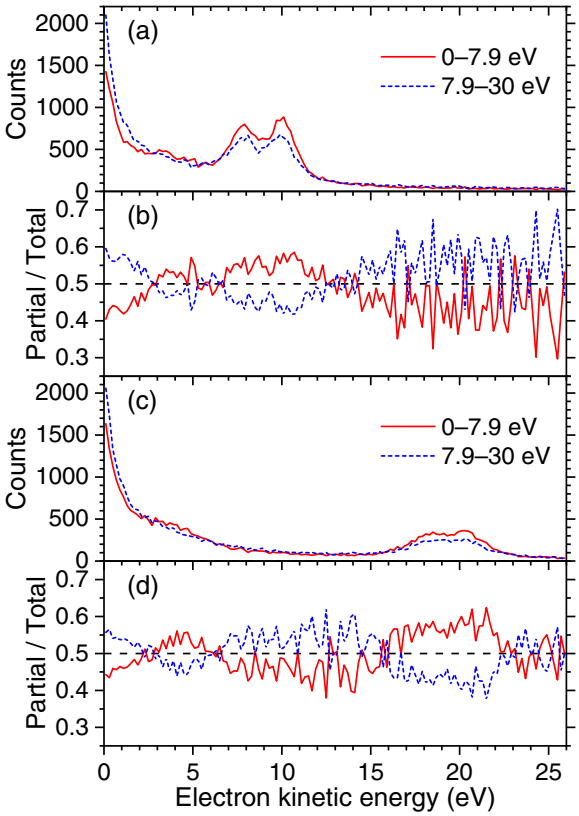

FIG. 5. Partial electron spectra at (a) 258-eV and (c) 268-eV photon energies separated by the sum of ion kinetic energies. Also shown are the ratios of the partial electron spectra to the total electron spectra at (b) 258 eV and (d) 268 eV. The bin size of the electron kinetic energy is 0.2 eV.

Figure 5 depicts partial electron spectra distinguished by the sum of three Ar^+ kinetic energies at the median energy (∼7.9 eV in Fig. 4). The ratios to the total electron spectrum for each photon energy are also shown. The partial electron spectra for high ion kinetic energy refer to the Ar cluster of which the charge state is mostly more than +3, while the ones for low ion kinetic energy are relevant to the Ar cluster whose charge state is mainly equal to +3. Similar trends are shown at both photon energies. Relative intensities due to the photoelectron peaks decrease, whereas those due to slope 1 [above the 15-eV region for 258 eV and above the (7–15)-eV region for 268 eV] and slope 2 [the (0–2)-eV region] increase when the sum of ion kinetic energies is high, i.e., the charge state of the Ar cluster is high. The Auger electrons have enough energy to cause inelastic scatterings several times, resulting in the creation of higher charge states. In addition, when both ICD or ETMD and the Auger inelastic scatterings occur, a charge state higher than +3 is created. Thus, it is consistent that slope 1 is enhanced when the charge state of the Ar cluster is high. Slope 2 is also enhanced when the charge state of the Ar cluster is high. This may indicate that the Auger inelastic scatterings also contribute to the production of the Rydberg states. There is another component in the (3–6)-eV region of which the behavior is different from slopes 1 and 2. The number of electrons due to ICD and ETMD processes depends not on the Auger electron inelastic scattering but

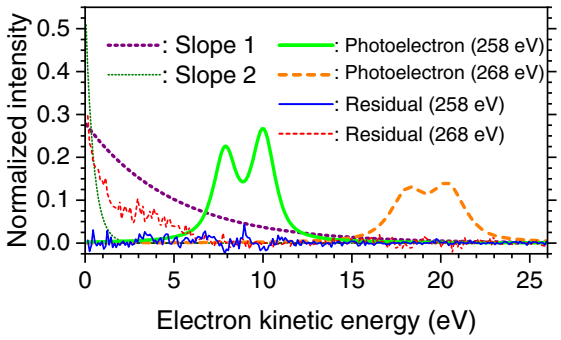

FIG. 6. Each component obtained from the fitting and subtraction for the electron spectra. Intensities are normalized, e.g., the integrated intensity of the photoelectrons around 10 eV is unity.

on the branching ratios to produce excited Ar^{2+} causing the ICD or ETMD. Thus, we consider it to be from ICD and/or ETMD.

For further investigation, in order to separate contributions from different origins and clarify differences between two spectra for clusters, we have performed curve-fitting analysis (see Appendix B for details). Figure 6 shows each component obtained from the fitting. The curves are extended to the electron-kinetic-energy regions that are not used to fit. Intensities are normalized in such a way that an integration of the photoelectron peaks in the 258-eV spectrum is unity. The 268-eV spectrum is normalized so that the intensities of both slopes are the same as those in the 258-eV spectrum. The residuals after subtracting the fitted curve are also shown. The integrated intensities are summarized in Table I.

It is noticeable that the photoelectron peak intensity in the 268-eV spectrum is smaller than that in the 258-eV spectrum, whereas residual intensities for 268 eV are much stronger than those for 258 eV. This may be considered a consequence of the photoelectron inelastic scattering by surrounding Ar atoms since the energy of photoelectrons emitted at 268-eV photon energy is higher than the excitation or ionization energy of Ar atoms. Namely, the kinetic energy of the photoelectron is used to excite or ionize another Ar atom in the cluster and thus the photoelectron is detected as an electron with kinetic energy lower than ∼20 eV. Thus, the difference between the residuals observed at 258 and 268 eV, 0.50 (= 0.54 − 0.04), is considered to be the number of the electrons originating from photoelectron inelastic scattering. We also consider that the residuals in the 258-eV spectrum originate from ICD and/or ETMD processes and thus 0.04 is the number of electrons from those processes.

Let us estimate branching ratios to produce electrons from those processes after Ar $2p$ photoionization. Table II shows the branching ratio for each process. Note that in order to obtain the branching ratios, photoelectrons emitted from clusters which were not observed in the experiment, i.e., photoelectrons in the events that release fewer than three ions, were considered. The probability that neither Auger electron inelastic scattering nor ICD or ETMD occur is 52%, as we will explain later. Thus, the observed photoelectrons are 48% of the Ar $2p$ photoelectrons emitted from the cluster. The intensities in Table I were multiplied by 0.48 and used

TABLE I. Integrated electron yield coincidence with three Ar^+ ions. Intensities for the photoelectron, slope 1, slope 2, and residual are obtained from the fitting analysis.

Photon energy (eV)	Photoelectron	Slope 1	Slope 2	Residual (<8 eV)
258	1.00	1.38 ± 0.04	0.25 ± 0.02	0.04 ± 0.01
268	0.75 ± 0.03	1.38 ± 0.04	0.25 ± 0.02	0.54 ± 0.05

to obtain the experimental branching ratios summarized in Table II.

Let us evaluate the validity of the branching ratios estimated for the processes listed in Table II. When we assume that the cluster is a sphere, using a solid Ar density of 1.65 g/cm^3 and cluster size of 70, we obtain that the radius of the cluster is 8.8 Å. We consider this distance as a representative distance by which the electron generated inside the cluster passes through the cluster. In the case of the 20-eV electron, using an electron impact excitation cross section of $\sim 6 \times 10^{-17}$ cm^2 [23] and an ionization cross section of $\sim 5 \times 10^{-17}$ cm^2 [24], the probabilities of the electron impact excitation and ionization are 12% and 10%, respectively. Thus, the number of the missing photoelectrons from the 20-eV peak is 22% (= 12% + 10%) and the number of electrons coming from photoelectron inelastic scattering is 32% (= 12% + 10% × 2) of the photoelectrons, where a factor of 2 in the second term comes from the fact that both scattered and ionized electrons contribute when electron impact ionization occurs.

Next, in the case of the Auger electron inelastic scattering, an Auger electron may multiply collide and ionize surrounding Ar atoms since the Auger electron has a kinetic energy of ~200 eV. Using the electron impact ionization cross section of the 200-eV electron $\sim 2 \times 10^{-16}$ cm^2 [24], the probability that electron impact ionization does not occur is ~65%. If we use the same cross sections for multiple collisions, the probabilities of collisional ionization which happens n ($n = 1$, 2, 3, and 4) times are 0.28, 0.061, 0.0089, and 0.000 97, respectively, from the Poisson distribution $P(n)$ in the case of $P(0) = 0.65$. When ionization happens n times, $n + 1$ electrons will be released. Thus, in total, the number of the electrons originating from Auger electron inelastic scattering is 79% of the Auger electrons.

Finally, in order for ICD to take place, Ar^{2+} produced via Auger decay (Fig. 1) needs to have enough energy to ionize surrounding neutral Ar. The energy of an excited Ar^{2+} state higher than $3s3p^5\,{}^1P$ is larger than the ionization energy of the neutral Ar atom [25]. Moreover, the energy of Ar^{2+} needs to overcome the Coulomb repulsion between the ICD products Ar^{2+} and Ar^+. In the case of the Ar dimer, the Coulomb repulsion energy is 7.8 eV, which is close to the energy calculated from the internuclear distance of the neutral Ar dimer [8]. In the present Ar clusters, the internuclear distance can be longer since the Coulomb interaction is a long-range interaction. When $Ar^{2+}(3s3p^5\,{}^1P)$ contributes to the ICD, for example, the distance between Ar^{2+} and Ar^+ is estimated to be longer than ~14 Å. This distance is smaller than the diameter of the Ar clusters in the present study and thus ICD may take place. In the case of the ETMD(3), since three participating species are required to be close to each other, we assume an internuclear distance of 3.8 Å from the neutral equilateral triangle Ar trimer [22]. In this case, the Coulomb repulsion energy between three Ar^+ ions is ~11 eV. The energy levels higher than $Ar^{2+}(3s3p^5\,{}^1P)$ [25] overcome this Coulomb repulsion energy and the ionization energy of two neutral Ar atoms. Thus ICD and/or ETMD(3) may take place for the Auger final Ar^{2+} states with the energy levels higher than $Ar^{2+}(3s3p^5\,{}^1P)$ and thus produce low-energy electrons. The branching ratio to populate those excited Ar^{2+} ions in those energy levels via Auger decay following Ar $2p$ ionization is ~20% [26] and thus the probability that ICD or ETMD does not occur is estimated to be ~80%. Multiplying the probabilities that electron impact ionization does not occur (~65%) and that ICD or ETMD does not occur (~80%), we obtain the probability that neither Auger electron inelastic scattering nor ICD or ETMD occurs (52% = 65% × 80%) and the normalization factor of 0.48 in Table II.

TABLE II. Branching ratios constructed from the experimental data in Table I and calculated using atomic data.

Process	Experiment	Calculation
Ar $2p$ photoionization in the cluster		1
produces three or more ions	0.48	0.48
produces less than three ions		0.52
missing photoelectrons[a]	0.12 ± 0.01	0.22
photoelectron inelastic scattering[a]	0.24 ± 0.02	0.32
Auger electron inelastic scattering	0.66 ± 0.02	0.79
ICD or ETMD	0.02 ± 0.01	0.20
autoionization	0.12 ± 0.01	

[a]The process is possible at 268-eV photon energy.

The calculated branching ratios as mentioned above are summarized in Table II. The calculated values are the ratio to the Ar $2p$ photoionization including both three or more ions productions and fewer than three ions productions. Thus, the normalization factor is not required. The branching ratio for the autoionization from vibrationally excited Rydberg states could not be estimated from the atomic data. The calculated values agree with experimental values within a factor of 2, except for the ICD or ETMD. The disagreement with the ICD or ETMD may come from an incomplete distinction between the Auger electron inelastic scattering and ICD or ETMD.

IV. SUMMARY

By performing electron-ion coincidence measurements, we experimentally identified the origins of the low-energy electrons emitted from Ar clusters as the inelastic scattering of the photoelectrons and Auger electrons with the surrounding and the interatomic electronic decay processes (ICD and/or ETMD) and we obtained their branching ratios. Evaluation

of these branching ratios based on the available atomic data gives semiquantitative agreement with the experimentally determined branching ratios. Our finding will help in the quantitative understanding of the radiation damage by low-energy electrons at the atomic level.

ACKNOWLEDGMENTS

The experiments were performed at the BL17SU of SPring-8 with the approval of the Japan Synchrotron Radiation Research Institute (Proposal No. 2014B1769). This study was supported by the X-ray Free Electron Laser Priority Strategy Program of the Ministry of Education, Culture, Sports, Science and Technology of Japan, by the Japan Society for the Promotion of Science KAKENHI Grant No. JP15K17487, by the Dynamic Alliance for Open Innovation Bridging Human, Environment and Materials, and by the IMRAM project.

H.F., Y.L., and D.Y. contributed equally to this work.

APPENDIX A: ESTIMATION OF CLUSTER SIZE

In the TIY spectrum measured at 1.5 MPa, structures not seen in the spectrum at 0.3 MPa appear (Fig. 2). These structures stem from clusters. For example, peaks at 244.7 and 245.2 eV stem from $2p_{3/2} \rightarrow 4s$ transitions of Ar on the surface and within the bulk of the argon clusters, respectively [20].

Assuming that the average number of atoms on the surface and within the bulk are proportional to the areas of the peaks from the surfaces and the bulks at 244.7 and 245.2 eV, we estimated the average number of atoms in the cluster (averaged cluster size $\langle N \rangle$). Namely, when the cluster has icosahedron geometry, the number of atoms on the surface (N_s), within the bulk (N_b), and in the cluster (N) are written as

$$N_s = 2(5m^2+1), \tag{A1}$$

$$N_b = \tfrac{1}{3}(2m-1)(5m^2-5m+3), \tag{A2}$$

$$N = \tfrac{1}{3}(2m+1)(5m^2+5m+3), \tag{A3}$$

where m is the number of layers of the cluster. Applying Eqs. (A1)–(A3) to the case that m is not an integer, we can estimate m from the ratio of the integrated peak intensities originating from the surface and bulk in the TIY spectrum and thus estimate cluster size using m. In order to estimate the ratio, we performed curve fittings to the TIY spectra as follows. First, the peak due to the $2p_{3/2} \rightarrow 4s$ transition at ~244.4 eV in the atomic spectrum (0.3 MPa) was fitted by a Lorentzian function. Then the cluster spectrum (1.5 MPa) around the $2p_{3/2} \rightarrow 4s$ transition region was fitted by two Gaussian functions and the Lorentzian function with the same center energy and width as obtained from the fitting for the atomic spectra. The estimated size is ~70 atoms per cluster. This size agrees with the size ~40 atoms per cluster obtained from the scaling law [27] within a factor of 2.

APPENDIX B: FITTING ANALYSIS FOR THE ELECTRON SPECTRA

In order to separate contributions of electrons from different origins in the electron spectra and clarify differences between two electron spectra for clusters measured at photon energies of 258 and 268 eV, we have performed curve-fitting analysis. We first fitted the model curve to the electron spectra of Ar atoms and reproduced the photoelectron peaks as described below. The observed peak shapes are broader than the lifetime broadening and thus are considered to reflect the instrumental function of the electron spectrometer. The instrumental function is a function of the electron kinetic energy and electron emission angle [28] and thus difficult to be formulated for the fitting analysis. Instead of formulating the function, we used two pseudo-Voigt functions in the fitting for the photoelectron peaks $I_{pe}(E)$,

$$\begin{aligned} I_{pe}(E) = A_1\Bigg[(1-\alpha_1)\frac{2\sqrt{\ln 2}}{w_1\sqrt{\pi}}\exp\left(-\frac{4\ln 2}{w_1^2}(E-E_1)^2\right) \\ +\alpha_1\frac{2}{\pi}\frac{w_1}{4(E-E_1)^2+w_1^2}\Bigg] \\ +A_2\Bigg[(1-\alpha_2)\frac{2\sqrt{\ln 2}}{w_2\sqrt{\pi}}\exp\left(-\frac{4\ln 2}{w_2^2}(E-E_2)^2\right) \\ +\alpha_2\frac{2}{\pi}\frac{w_2}{4(E-E_2)^2+w_2^2}\Bigg] + \text{const}, \end{aligned} \tag{B1}$$

because it reproduces the measured peaks. Here E is electron kinetic energy and A_i, α_i, w_i, and E_i ($i = 1, 2$) are parameters.

For the fitting to the cluster spectra, other components for slope 1 and slope 2 are required. Thus, the sum of two exponential distributions was introduced for the fitting to the cluster spectra $I_{cluster}(E)$,

$$\begin{aligned} I_{cluster}(E) = I_{pe}(E) + B_1\exp(-k_1E) \\ + B_2\exp(-k_2E) + \text{const}, \end{aligned} \tag{B2}$$

where B_i and k_i ($i = 1, 2$) are parameters. In the fitting to the cluster spectra α_i and w_i are fixed as those obtained from the fitting for the atomic spectra, whereas A_i and E_i are treated as fitting parameters. We first performed the fitting to the spectrum measured at 258-eV photon energy. An electron-kinetic-energy region between 2 and 7 eV is ignored in the fitting because the fitting analysis tells us there are components which are not included in the fitting function. This energy region is close to the energy of the ICD electrons emitted from Ar dimers [8] and trimers [9]. For the spectrum measured at 268-eV photon energy, the slopes with the same shape, i.e., with the same B_1/B_2 ratio, k_1 and k_2, as those obtained from the fitting for the 258-eV spectrum were used and the electron-kinetic-energy region below 7 eV was ignored in the fitting.

[1] W. Bambynek, B. Crasemann, R. W. Fink, H.-U. Freund, H. Mark, C. D. Swift, R. E. Price, and P. V. Rao, X-ray fluorescence yields, Auger, and Coster-Kronig transition probabilities, Rev. Mod. Phys. **44**, 716 (1972).

[2] B. Boudaïffa, P. Cloutier, D. Hunting, M. A. Huels, and L. Sanche, Resonant formation of DNA strand break by low-energy (3 to 20 eV) electrons, Science **287**, 1658 (2000).

[3] L. S. Cederbaum, J. Zobeley, and F. Tarantelli, Giant Intermolecular Decay and Fragmentation of Cluster, Phys. Rev. Lett. **79**, 4778 (1997).

[4] V. Averbukh, P. V. Demekhin, P. Kolorenc, S. Scheit, S. D. Stoychev, A. I. Kuleff, Y.-C. Chiang, K. Gokhberg, S. Kopelke, N. Sisourat, and L. D. Cederbaum, Interatomic electronic decay processes in singly and multiply ionized clusters, J. Electron Spectrosc. Relat. Phenom. **183**, 36 (2011).

[5] T. Jahnke, Interatomic and intermolecular Coulombic decay: The coming of age story, J. Phys. B **48**, 082001 (2015).

[6] T. Jahnke, H. Sann, T. Havermeier, K. Kreidi, C. Stuck, M. Meckel, M. Schöffler, N. Neumann, R. Wallauer, S. Voss, A. Czasch, O. Jagutzki, A. Malakzadeh, F. Afaneh, T. Weber, H. Schmidt-Böcking, and R. Dörner, Ultrafast energy transfer between water molecules, Nat. Phys. **6**, 139 (2010).

[7] M. Mucke, M. Braune, S. Barth, M. Förstel, T. Lischke, V. Ulrich, T. Arion, U. Becker, A. Bradshaw, and U. Hergenhahn, A hitherto unrecognized source of low-energy electron in water, Nat. Phys. **6**, 143 (2010).

[8] Y. Morishita, X.-J. Liu, N. Saito, T. Lischke, M. Kato, G. Prümper, M. Oura, H. Yamaoka, Y. Tamenori, I. H. Suzuki, and K. Ueda, Experimental Evidence of Interatomic Coulombic Decay from the Auger Final States in Argon Dimers, Phys. Rev. Lett. **96**, 243402 (2006).

[9] X.-J. Liu, N. Saito, H. Fukuzawa, Y. Morishita, S. Stoychev, A. Kuleff, I. H. Suzuki, Y. Tamenori, R. Richter, G. Prümper, and K. Ueda, Evidence of sequential interatomic decay in argon trimers obtained by electron–triple-ion coincidence spectroscopy, J. Phys. B **40**, F1 (2007).

[10] N. Saito, Y. Morishita, I. H. Suzuki, S. D. Stoychev, A. I. Kuleff, L. S. Cederbaum, X.-J. Liu, H. Fukuzawa, G. Prümper, and K. Ueda, Evidence of radiative charge transfer in argon dimers, Chem. Phys. Lett. **441**, 16 (2007).

[11] K. Kreidi *et al.*, Relaxation processes following 1*s* photoionization and Auger decay in Ne_2, Phys. Rev. A **78**, 043422 (2008).

[12] J. Zobeley, R. Santra, and L. S. Cederbaum, Electron decay in weakly bound heteroclusters: Energy transfer versus electron transfer, J. Chem. Phys. **115**, 5076 (2001).

[13] V. Stumpf, P. Kolorenč, K. Gokhberg, and L. S. Cederbaum, Efficient Pathway to Neutralization of Multiply Charged Ions Produced in Auger Processes, Phys. Rev. Lett. **110**, 258302 (2013).

[14] D. You *et al.*, Charge transfer to ground-state ions produces free electrons, Nat. Commun. **8**, 14277 (2017).

[15] M. Oura, T. Nakamura, T. Takeuchi, Y. Senba, H. Ohashi, K. Shirasawa, T. Tanaka, M. Takeuchi, Y. Furukawa, T. Hirono, T. Ohata, H. Kitamura, and S. Shin, Degree of circular polarization of soft x-rays emitted from a multi-polarization-mode undulator characterized by means of magnetic circular dichroism measurements, J. Synchrotron Radiat. **14**, 483 (2007).

[16] R. Dörner, V. Mergel, O. Jagutzki, L. Spielberger, J. Ullrich, R. Moshammer, and H. Schmidt-Böcking, Cold target recoil ion momentum spectroscopy: A 'momentum microscope' to view atomic collision dynamics, Phys. Rep. **330**, 95 (2000).

[17] J. Ullrich, R. Moshammer, A. Dorn, R. Dörner, L. P. H. Schmidt, and H. Schmidt-Böcking, Recoil-ion and electron momentum spectroscopy: Reaction-microscopes, Rep. Prog. Phys. **66**, 1463 (2003).

[18] K. Ueda, H. Fukuzawa, X.-J. Liu, K. Sakai, G. Prümper, Y. Morishita, N. Saito, I. H. Suzuki, K. Nagaya, H. Iwayama, M. Yao, K. Kreidi, M. Schöffler, T. Jahnke, S. Schössler, R. Dörner, T. Weber, J. Harries, and Y. Tamenori, Interatomic Coulombic decay following the Auger decay: Experimental evidence in rare-gas dimers, J. Electron Spectrosc. Relat. Phenom. **166–167**, 3 (2008).

[19] M. Kato, Y. Morishita, M. Oura, H. Yamaoka, Y. Tamenori, K. Okada, T. Matsudo, T. Gejo, I. H. Suzuki, and N. Saito, Absolute photoionization cross sections with ultra-high energy resolution for Ar, Kr, Xe and N_2 in inner-shell ionization regions, J. Electron Spectrosc. Relat. Phenom. **160**, 39 (2007).

[20] O. Björneholm, F. Federmann, F. Fössing, and T. Möller, Core Level Photoelectron and X-Ray Absorption Spectroscopy of Free Argon Clusters: Size-Dependent Energy Shifts and Determination of Surface Atom Coordination, Phys. Rev. Lett. **74**, 3017 (1995).

[21] C. Dimopoulou, R. Moshammer, D. Fischer, C. Höhr, A. Dorn, P. D. Fainstein, J. R. C. L. Urrutia, C. D. Schröter, H. Kollmus, R. Mann, S. Hagmann, and J. Ullrich, Breakup of H_2 in Singly Ionizing Collisions with Fast Protons: Channel-Selective Low-Energy Electron Spectra, Phys. Rev. Lett. **93**, 123203 (2004).

[22] T. González-Lezana, J. Rubayo-Soneira, S. Miret-Artés, F. A. Gianturco, G. Delgado-Barrio, and P. Villarreal, Comparative configurational study for He, Ne, and Ar trimers, J. Chem. Phys. **110**, 9000 (1999).

[23] A. Chutjian and D. C. Cartwright, Electron-impact excitation of electronic states in argon at incident energies between 16 and 100 eV, Phys. Rev. A **23**, 2178 (1981).

[24] H. Tawara and T. Kato, Total and partial ionization cross sections of atoms and ions by electron impact, At. Data Nucl. Data Tables **36**, 167 (1987).

[25] A. Kramida, Y. Ralchenko, J. Reader, and NIST ASD Team, NIST Atomic Spectra Database, version 5.5.6, 2018, available at https://physics.nist.gov/asd.

[26] H. Pulkkinen, S. Aksela, O.-P. Sairanen, A. Hiltunen, and H. Aksela, Correlation effects in the $L_{2,3}$-MM Auger transitions of Ar, J. Phys. B **29**, 3033 (1996).

[27] U. Buck and R. Krohne, Cluster size determination from diffractive He atom scattering, J. Chem. Phys. **105**, 5408 (1996).

[28] T. Jahnke, T. Weber, T. Osipov, A. L. Landers, O. Jagutzki, L. P. G. Schmidt, C. L. Cocke, M. H. Prior, H. Schmidt-Böcking, and R. Dörner, Multicoincidence studies of photo and Auger electrons from fixed-in-space molecules using COLTRIMS technique, J. Electron Spectrosc. Relat. Phenom. **141**, 229 (2004).